

UC Davis

UC Davis Previously Published Works

Title

Cellulose and Lignocellulose Nanofibrils and Amphiphilic and Wet-Resilient Aerogels with Concurrent Sugar Extraction from Almond Hulls

Permalink

<https://escholarship.org/uc/item/7c56434z>

Journal

ACS Agricultural Science & Technology, 3(1)

ISSN

2692-1952

Authors

Patterson, Gabriel D
Orts, William J
McManus, James D
[et al.](#)

Publication Date

2023-01-16

DOI

10.1021/acsagscitech.2c00264

Copyright Information

This work is made available under the terms of a Creative Commons Attribution License, available at <https://creativecommons.org/licenses/by/4.0/>


Peer reviewed

Cellulose and Lignocellulose Nanofibrils and Amphiphilic and Wet-Resilient Aerogels with Concurrent Sugar Extraction from Almond Hulls

Gabriel D. Patterson, William J. Orts, James D. McManus, and You-Lo Hsieh*

 Cite This: *ACS Agric. Sci. Technol.* 2023, 3, 140–151 Read Online

ACCESS |

 Metrics & More Article Recommendations

ABSTRACT: With downward pressure on the value of almond hulls (AHs), the major byproduct from the largest tree nut crop globally, the streamlined production of several grades of cellulose nanofibrils (CNFs) toward novel aerogels with concurrent sugar extraction was introduced to synergistically drive these products toward commercial adoption. Hot water extraction produced 50% lignocellulose (LC) with equal water-soluble sugars from AH of a soft-shell variety. Aqueous NaOH and NaClO₂/KOH treatments isolated ca. 15% alkali cellulose and 12% cellulose, respectively. Coupled 2,2,6,6-tetramethylpiperidine-1-oxyl (TEMPO) oxidation and blending yielded 88, 91, and 95% LC micro-/nanofibrils (LCMNFs), alkali cellulose nanofibrils (ACNFs), and cellulose nanofibrils (CNFs) with, respectively, 0.76, 1.02, and 0.84 mmol/g surface carboxyls in a similar 4:1 width-to-thickness aspect ratio and ultrahigh length-to-thickness aspect ratios (800–1900). The LCMNF aerogel was mostly wet-resilient, wet-stable, and dry/wet shape-recoverable, whereas the most charged ACNFs gave the stiffest aerogel [31.6 kPa/(mg/cm³)].

KEYWORDS: almond hull, cellulose nanofibrils, aerogels, lignin-containing, concurrent extraction, free sugars

INTRODUCTION

Cellulose, nature's most-abundant polymer,¹ has been the basis of paper and textile industries for millennia because of its availability and remarkable versatility afforded by its physical and chemical properties. Recently, there has been a tremendous effort to commercialize the production and application of nanocelluloses, the relatively crystalline nanoscale materials derived from plants, bacteria, and marine animals. The widths and lengths of nanocelluloses range from a few nanometers to micrometers, with shapes ranging from rod-like cellulose nanocrystals (CNCs) to significantly longer cellulose nanofibrils (CNFs).

Nanocellulose materials hold tremendous promise because, for example, they are “stronger than steel” on a per weight basis when acting as reinforcing agents.² Nanocrystals can readily self-assemble into an array of highly organized liquid crystalline structures³ and can be safely used in medical applications as both a drug carrier and for structural remediation,^{4,5} and when modified to become electroconductive,⁶ CNCs can be envisioned for use in organic microcircuits or “smart clothing,” considering that they align in magnetic fields.⁷

Despite all these promising developments and clear potential, nanocellulose production has yet to scale up to the level where large quantities are available at predictable, stable prices. Part of the drawback is the need to isolate these nanocelluloses from relatively pure sources of cellulose and the resultant relatively low yield due to the harsh extraction conditions to achieve relative purity. Thus, as a “stand-alone” process, nanocellulose production has not taken off. Therefore, cellulose isolation/extraction and generating nanocelluloses

from less-purified feedstock alongside valuable coproducts is an essential consideration.

The production of tree nut crops has increased nearly 10-fold in the past 20 years, with almonds being the largest of all tree nut crops at 31% of the global share and 1.65 million metric tons in 2020/2021, representing an 18% increase in production tonnage from the previous year.^{8,9} California contributes over 85% of the global almond production^{9–11} and, as a result, generates an increasing fraction of underutilized byproducts—the shells and the hulls—at nearly 3 times the dry weight of the kernels. Specifically available beyond the kernels are 53.5% woody biomass (dead trees, tree prunings, and shells) and 46.5% sugar-rich, fleshy, and underutilized almond hull (AH).¹²

At approximately a 2:1 mass ratio to the kernel, AHs constitute the largest byproduct. They represent billions of pounds annually of lignocellulosic biomass with limited use, mainly as supplemental feed to dairy cows^{13–20} but could be valorized for higher-value end uses. Importantly, AHs have up to 60 wt % (by dry mass) water-soluble extractables,²¹ including nearly 50 wt % sugars,²² such as fermentable sugars (glucose, fructose, and sucrose) and sugar alcohols (inositol and sorbitol) as “free sugars.” These sugars are of high value to

Received: September 30, 2022

Revised: December 2, 2022

Accepted: December 2, 2022

Published: December 23, 2022



the feed and food industries. With the declining numbers of dairies in California,²³ almond researchers have explored new uses, including feed for broiler chickens,²⁴ larvae-based animal feeds, desugared “spent hull” as a soil amendment,²⁵ free sugars for fermentation and natural sweeteners,^{22,26} and for extraction of phenolic antioxidants for nutraceutical uses.^{27–29} From stepwise forage analysis, AHs have been reported to contain 6.6–15.5 wt % cellulose and 6–10 wt % hemicellulose,^{16–20,22,25} 24.3–54.5 wt % nonfibrous carbohydrate,^{7,19,25} and 4.4–12.3 wt % acid-detergent lignin.^{17–20,22,25} Therefore, the sugar-rich and fleshy AH is an excellent source of both high-value commodity sugars and lignocellulosic biomass for value-added material applications.

Nanocelluloses have most commonly been produced from wood pulp.³⁰ Recently, the list of nanocelluloses from lignocellulosic biomass has expanded significantly to include coconut husk,³¹ cotton linter,³² grape skin,³³ tomato peel,³⁴ rice straw,^{35–37} ginger fiber wastes,³⁸ sugarcane bagasse,^{39,40} corn husks,⁴¹ almond shell,⁴² hop stems,⁴³ and numerous other agricultural crop residues and byproducts. Finding applications for such unutilized or under-utilized biomass is increasingly recognized to reduce greenhouse gas (GHG) outputs by, first, preventing these feedstocks from ending up in waste streams where they could decompose into methane, a very potent GHG. Adding value to these under-utilized lignocellulosic resources with potentially new applications of nanocelluloses will be described in this report, providing the opportunity to go “up the value chain” toward higher-value commercial uses. The sheer quantity of annually available, already-collected, and mostly under-utilized AHs presents significant opportunities for new nanocellulose-based material developments.

This study provides critical insight into isolating CNFs from AHs by exploring three different isolation procedures that result in various lignocellulose (LC) to cellulose-rich fractions for improved AH utilization. Given the remarkably high free sugar levels (ca. 50 wt %) and relatively low cellulose content (<16 wt %) of AHs, developing high value-added nanocelluloses is promising when coupled with sugar extraction from this significant almond byproduct.

To explore final end uses for these nanocellulose products from AHs, all three AH isolates were subjected to an optimized 2,2,6,6-tetramethylpiperine-1-oxyl radical (TEMPO)-mediated oxidation (5 mmol NaClO/g) coupled with high-speed mechanical blending³⁶ to study how the quantities and qualities (dimensions, surface chemistries, and charges) of the CNFs produced are impacted by the presence of noncellulosics or the cellulose purity of the isolates. These CNFs were self-assembled into aerogels by a freeze/freez-dry procedure⁴⁴ to investigate the effects of the CNF qualities and purities, that is, the presence of lignin and hemicelluloses, on the hierarchical structures and mechanical and functional properties of the aerogels. The goal is to understand how isolation process optimization affects nanocellulose production and product performance toward significant added value to the under-utilized AH.

Hypotheses. (1) Streamlined LC to cellulose isolation processes concurrently and synergistically produce water-soluble and fermentable sugars from AHs as parallel coproducts for full utilization. (2) The purity of the LC to cellulose-rich isolates dictates the qualities and quantities of the CNFs by a coupled TEMPO/blending chemical-mechanical process, which influence the properties of the self-assembled aerogels.

EXPERIMENTAL SECTION

Materials. AHs were from a soft-shell Carmel variety grown in California. Sodium chlorite (NaClO₂, 80%, Fluka), glacial acetic acid (CH₃COOH, 99.7%, ACS GR, EMD), potassium hydroxide (KOH, 85%, EM Science), sodium hydroxide (NaOH, 97%, Sigma-Aldrich), sodium hypochlorite solution (NaClO, 11.9%, reagent grade, Sigma-Aldrich), TEMPO (99.9%, Sigma-Aldrich), sodium bromide (NaBr, BioXtra, 99.6%, Sigma-Aldrich), sodium hydroxide (NaOH, 1 N, Certified, Fisher Scientific), hydrochloric acid (HCl, 1 N, Certified, Fisher Scientific), chloroform (HPLC grade, EMD), and decane (Certified ACS, Fisher Scientific) were used as received. All water used is from the Milli-Q plus water purification system (Millipore Corporate, Billerica, MA).

Isolation of Cellulose, Alkali Cellulose, and LC. AHs were dried (50 °C, overnight), milled (60-mesh, 0.25 mm, Thomas-Wiley Laboratory Mill model 4, Thomas Scientific, USA), and redried (2 days, 50 °C). Simple hot water extraction (70 °C, 30 min) of AH powders (40.0 g) removed sugars and other water solubles, even though presumably not lignin. An aqueous 4% NaOH alkali treatment (70 °C, 5 min, twice)⁴⁵ was applied to isolate cellulose-containing lower lignin levels, or “alkali cellulose”. A three-step isolation followed a previous report on rice straw,³⁵ that is, organic solvent dewaxing with 2:1 toluene/ethanol v/v (300 mL, 20 h), then delignified in 1 L of acidified 1.4% NaClO₂ (CH₃COOH, pH 3.5, 70 °C, 5 h, 600 rpm), and last treated in 5% KOH (600 mL, RT, 24 h: 90 °C, 2 h). The three-step process was reduced to a two-step NaClO₂/KOH dissolution to isolate “aqueous cellulose” by omitting organic extraction. All isolates were dried by freezing (−196 °C, 15 min), followed by freeze-drying (−50 °C, 0.05 mbar, FreeZone 1.0 L Benchtop Freeze Dry System, Labconco, Kansas City, MO) and then solid-state characterizations and coupled chemical/mechanical defibrillation.

Synthesis of CNFs. Heterogeneous and regioselective TEMPO-mediated oxidation was conducted in conjunction with isolation and, for comparative purposes, in parallel with the formation of dried isolates (1 g) in water (100 mL). Oxidation was achieved using 0.016 g of TEMPO catalyst, 0.1 g of NaBr cocatalyst, and 5.0 mmol/g of NaClO oxidant and maintained at a pH of 10 ± 0.2 (0.5 M NaOH).³⁶ Each reaction was ended once the pH ceased to decrease to record the reaction times and neutralized to pH 7.5 (0.5 N HCl) and dialyzed against water (12–14 kDa, ~48 h) until the filtrate was <10 μS/cm or a pH of 5.7. The TEMPO-oxidized solids were blended (37.5 k rpm, 30 min, Vitamix 5200), and the CNF-containing aqueous supernatants were collected (5k rpm, 15 min, Thermo Fisher Scientific, Megafuge 1.6 L) for determination of gravimetric yield and characterizations.

Characterization of Aqueous CNFs. The various C6-carboxylated CNF samples isolated from the different cellulose-containing sources had the total surface charges quantified by acid–base conductometric titration (OAKTON pH/Con 510). From each nanofibril-containing supernatant was prepared a 50 mL of aliquot at 0.05 w/v %. To each aliquot was added 200 μL of sodium chloride (NaCl, 0.5 M) to raise the conductivity and 50 μL of hydrochloric acid (HCl, 1 N) to fully convert the surface carboxylates (COO[−]) to carboxylic acids (COOH). Titration of each aliquot was conducted in parallel using 0.01 N NaOH. The total COOH [σ , in mmol/g, or mol/mol COOH/anhydroglucose unit (AGU), $M = 162$ g/mol] was calculated using

$$\sigma = \frac{c\Delta v}{m} = \frac{c(v_2 - v_1)}{m} \quad (1)$$

where c is the NaOH concentration (M), v_1 and v_2 are the NaOH volume (mL) used to neutralize added free HCl and surface COOH groups, respectively, and m is the CNF mass (g) in suspension. Conversely, the as-is ratio of surface COO[−]/COOH on nanofibrils at pH 5.7 was determined indirectly by titration without added acid. Any consumption of NaOH was attributable to surface COOH already present.

Table 1. Properties of TEMPO-Oxidized Nanocelluloses from Various AH Isolates

Isolation				TEMPO/blending + centrifugation		
Isolate	Process	Advantages	Mass of AH (%)	TEMPO oxidation time (min)	NCs in supernatant (5k rpm centrifugation) (%)	Mass of AH (%)
Lignocellulose	Hot water (70 °C, 30 min)	Aqueous sugar-rich effluent	51.4	30-45	88 (<i>n</i> =1) <i>microfibrils</i> : 82%	45.2
Alkali cellulose	Hot alkali (4 % NaOH, 70 °C, 5 min, twice)	One-step, rapid extraction of most non-cellulosics	15.0	45-60	91 ±5.3 (<i>n</i> =2)	13.7
Aqueous cellulose	Hot NaClO ₂ /KOH (1.4 % NaClO ₂ , 70 °C, 5 h /5 % KOH, 90 °C, 2h)	Two-step purified cellulose	11.7	90	95 ±1.7 (<i>n</i> =5)	11.1
Organic-extracted cellulose	2:1 toluene/ethanol, Hot NaClO ₂ /KOH as above	Three-step purified cellulose with little gain in yield	12.1	90	97 (<i>n</i> =1)	11.7

The atomic force microscope was a scanning probe system (Asylum-Research MFP-3D, Igor Pro 6.21) comprising a standard silicon cantilever (OMCL-AC160TS). A 10 μL drop of each nanofibril supernatant (0.0005 w/v %) was deposited on fresh flat surfaces of hydrophilic mica substrates and dried at room temperature (10–15 min). Then, the dried nanofibrils on the mica substrates were observed using tapping-mode AFM at a fixed 1 Hz scan rate. The thicknesses (*T*) of CNFs, ACNFs, and LCNFs were determined from 124, 70, and 35 individual nanofibrils, respectively, and the lengths (*L*) were estimated from 44, 19, and 19 individual nanofibrils, respectively. Welch's *T*-tests ($\alpha = 0.05$) of unequal variance were applied for the statistical comparison of the means.

To complete the characterization of the basic morphological parameters of the CNFs, a 10 μL drop of supernatant (0.0005 w/v %) was deposited onto freshly glow-discharged formvar carbon grids (300-mesh copper, Ted Pella Inc., Redding, CA) for transmission electron microscopy (TEM) (JEOL 1230, 100 kV). Excess solution was blotted with a filter paper, and the nanofibrils stained negatively with 2 w/v % uranyl acetate before being allowed to dry. The widths (*W*) of oCNFs and CNFs were determined from 63 and 98 individual nanofibrils.

Additional characterization of the various nanofibril supernatants included polarized light microscopy and transmittance using a UV–vis spectrophotometer ($\lambda = 300\text{--}800$ nm, Evolution 600).

Solid-State Characterizations of CNFs. The raw material isolates and 0.1 w/v % aliquots from each aqueous supernatant were rapidly frozen (-196 °C, liquid N₂) and then lyophilized (-50 °C, 24 h) in a freeze-dryer (FreeZone 1.0 L Benchtop Freeze Dry Systems, Labconco, Kansas City, MO). Each freeze-dried fibrous mass was used for (1) Fourier transform infrared spectroscopy (FTIR) (Nicolet 6700, Thermo Scientific, 1:100 w/w ratio to KBr, RT, 4 cm^{-1} resolution, 128 scans) and (2) thermal gravimetric analysis (TGA) (TGA-50, Shimadzu, Japan) using 5–10 mg of sample at 10 °C/min under constant flowing N₂ (50 mL/min) and RT–600 °C. Only the original AH powder, aqueous extracted cellulose, and the corresponding CNFs were subjected to X-ray diffraction (XRD) (Panalytical powder XRD, Ni-filtered Cu *K* α radiation, $\lambda = 0.1548$ nm) recorded from 10–30° 2 θ diffraction angle at 45 kV and 40 mA. The crystallinity index (CrI, %) was calculated using the maximum intensity of the 200 crystallographic lattice peak (*I*₂₀₀) at 22.7° and the minimum intensity (*I*_{am}) between the 200 and 110 peak at 18.7° by the following Segal equation:⁴⁶

$$\text{CrI} = \left(\frac{I_{200} - I_{am}}{I_{200}} \right) \times 100 \quad (2)$$

Assuming a rhomboidal cross-section of CNFs,⁴⁷ wherein the widths (*W*) and thicknesses (*T*) corresponded to the hydrophilic 110 and hydrophobic 200 crystal lattice planes, respectively, and only accessible surface AGUs on crystalline surfaces, the concentration of exposed primary C6 hydroxyl groups (ϕ , mol/mol) was calculated as

$$\phi = 2 \times \left[\frac{\frac{W}{d_{110}}}{\left(\frac{W}{d_{110}} + 1 \right) \times \left(\frac{T}{d_{110}} + 1 \right)} \right] \quad (3)$$

where *d*₁₁₀ and *d*₁₁₀ are 0.53 and 0.61 nm *d*-spacings from the 2 θ diffraction peaks at 16.8 and 14.7°, respectively.

CNF Aerogel Fabrication and Characterizations. All supernatants were simultaneously concentrated and degassed using a rotary evaporator. Approximately, 6 mL of 0.6 w/v % aliquots was pipetted into Pyrex glass tubes (1.4 cm wide and 5.5 cm height) before freezing (-20 °C, overnight) to form a cryogel, which were then freeze-dried (-50 °C, 0.05 mbar) into aerogels.

The density of each cylindrically shaped aerogel (ρ_a , mg/cm³) was calculated following the determination of the diameter (cut to 1.0 cm height) using a digital caliper (0.01 cm resolution) and the weight (0.1 mg resolution). The porosity (ϕ , %) was calculated as

$$\phi = \left(1 - \frac{\rho_a}{\rho_c} \right) \times 100 \quad (4)$$

where ρ_c is the density of crystalline cellulose (1.6 g/cm³).⁴⁸ The pore volume (cm³/g), also expressed as the absorption capacity (mL/g), was calculated as

$$\text{Capacity} = \frac{\phi}{\rho_a} \quad (5)$$

A one-way analysis of variance (ANOVA) ($\alpha = 0.05$) was applied for the statistical comparison of the means of the density, porosity, and absorption capacity of the aerogels. The measured absorption (mL/g) of water and decane was determined by weighing each aerogel in the dry state (*w*₀) and the fully saturated state (*w*_s), or

$$\text{Absorption} = \left(\frac{w_s - w_0}{w_0} \right) \div \rho_l \quad (6)$$

where ρ_l is the liquid density (g/mL). The absorption percentage (%) of the aerogel was calculated as

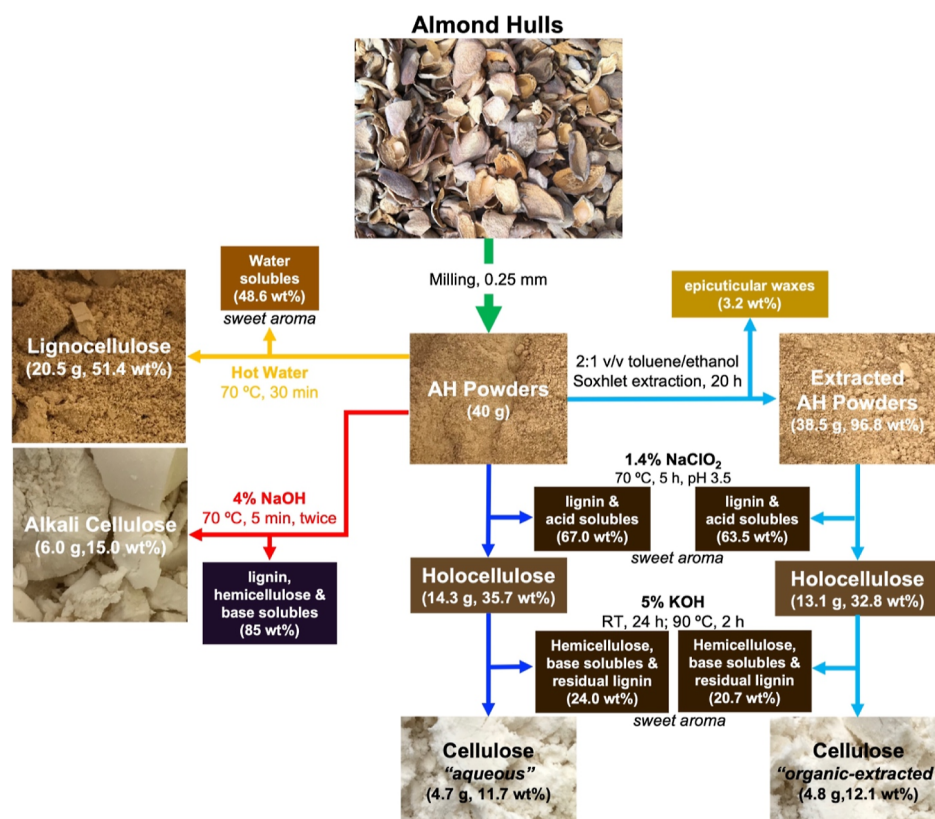


Figure 1. Scheme for organic-extracted cellulose, aqueous cellulose, alkali cellulose, and LC isolations from AHs. All yield values (wt %) are based on the original dry mass of AH.

Absorption percentage

$$= (\text{measured absorption} \div \text{capacity}) \times 100\% \quad (7)$$

and was indicative of the aerogel cellular structure (open vs. closed). Specifically, the cellular structure of the aerogels was characterized by imaging of 1 mm radial cross-sections placed on glass slides for light microscopy and fixed onto conductive carbon tape and gold sputter-coated for scanning electron microscopy (SEM) (SEM QUATTRO Environmental S, Thermo Scientific, 5 kV, 10 mm working distance). Compressive tests were performed on 1 cm tall aerogels using an Instron 5566 equipped with a 5 kN load cell and constant 1 mm/min loading–unloading rates. Compressions in the air were at 21 °C and 65% relative humidity, and compressions in the water were conducted inside a glass container at pH 5.7. The specific Young's modulus [E_p , kPa/(mg/cm³)] of each aerogel was normalized by its density and calculated from the slope of the linear elastic regime of the stress–strain curves.

RESULTS AND DISCUSSION

Isolation of LC and Celluloses from AHs. Milled AH powders were light brown in color, as expected from the presence of lignin chromophores and more than a dozen other phenolic antioxidants or glycosylated flavonoids.^{27–29} Hot water extraction (70 °C, 30 min) of AH powders removed 48.6 wt % water solubles as a brown and aromatic effluent and an insoluble 51.4 wt % “LC” isolate (Table 1), similar to the 46.3 wt % water-soluble sugars of Nonpareil AHs outlined by Holtman et al.²² making this hot water-alone extraction most compatible with sugar-removal processes for LC.

The two-time sodium hydroxide extraction (4% NaOH, 70 °C) documented for simultaneous and substantial removal of both water solubles and insoluble noncellulosics (hemicelluloses and lignin) from rice straw⁴⁵ gave a deep brown to

purple/black effluent and yielded a 15 wt % off-white “alkali cellulose” presumably containing minimum lignin (Figure 1). Alternatively, in the two-step NaClO₂ and KOH extraction, acidified 1.4% NaClO₂ treatment (70 °C) removed 67.0 wt % mass in a deep brown effluent with a sugary aroma and gave a dark brown isolate. Note that NaClO₂ decomposes to chlorine dioxide (NaClO₂ + CH₃COOH → ClO₂ + CH₃COONa + H⁺),^{48,49} which is effective in oxidizing phenolic, allylic methyl, or methylene lignin groups,^{49,50} and so, this significant mass loss in the effluent likely contained lignin as well as acid solubles and water solubles. Subsequent leaching with 5% KOH (90 °C) removed another 24.0 wt % of, presumably, hemicelluloses and possibly residual lignin and base-soluble polyphenols in a deep brown sugary aroma effluent and yielded a 11.7 wt % white/off-white relatively pure “aqueous cellulose”.

Soxhlet organic extraction of AH powders removed 3.2 wt % epicuticular waxes to give 96.8 wt % organic-extracted AH without a change in color (Figure 1). Ultimately, “organic-extracted cellulose” was isolated at 12.1 wt % (0.4 wt % higher) with similar white/off-white color after removing 63.5 wt % mass by NaClO₂ and 20.7 wt % mass by KOH. These two different NaClO₂/KOH isolation procedures were important to explore because, previously, extracting epicuticular waxes before aqueous pretreatment of grape skins, rice straw, and tomato peels produced the purest form of cellulose for nanocellulose production.^{33–35} While the 1.7–3.3 wt % wax contents of hulls are similarly low,^{16,18,20} the ca. 12 wt % yields of cellulose with and without organic extraction (12.1 vs 11.7 wt %) suggest that the dewaxing step is superfluous. More significantly, omitting this dewaxing step avoids the use of the less environmentally friendly organic solvents.

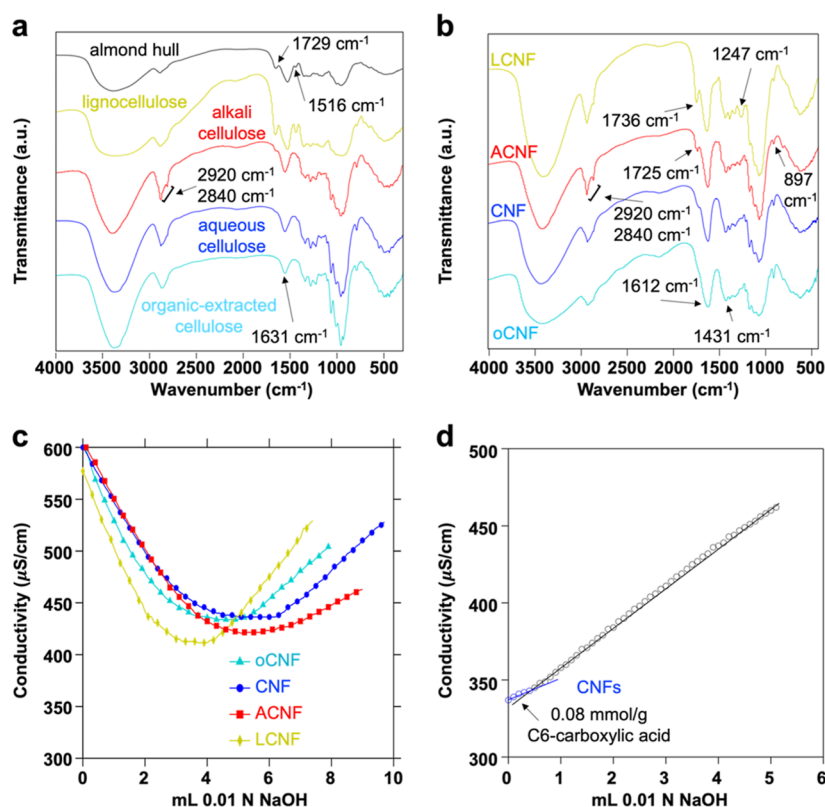


Figure 2. AH isolates and CNFs: (a,b) FTIR; (c) conductometric titration of aqueous CNF supernatants; and (d) titration of surface carboxyls without added acid.

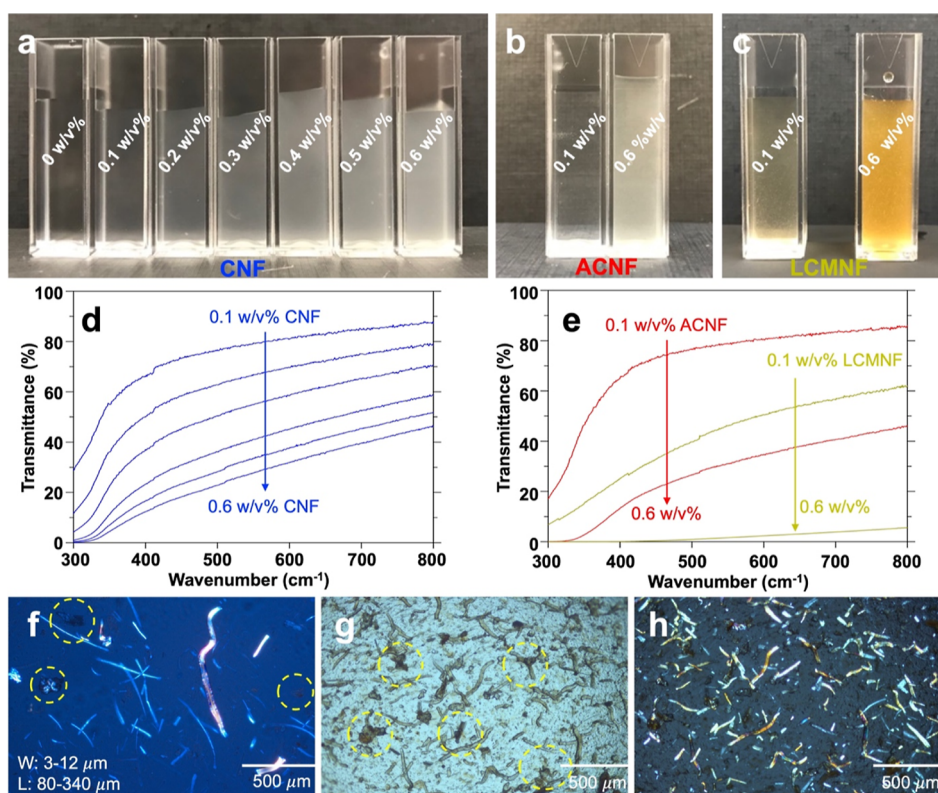


Figure 3. Visual appearances of aqueous supernatants of (a) CNFs, (b) ACNFs, and (c) LCMNFs; UV-vis transmittance of (d) CNFs and (e) ACNFs and LCMNFs; optical microscopy images of LCMNFs at 0.6 w/v% as (f) supernatant under cross-polar (yellow circles indicating lignin) and (g) oven-dried film (50 $^{\circ}\text{C}$, 24 h) under transmission and (h) oven-dried film under cross-polar.

Table 2. Comparison of CNFs and Their Aerogel Properties

Nanofibril properties				Aerogel properties		Water absorption		Decane absorption		Dry mechanical properties		Wet mechanical properties	
Sample ^a	Carboxyl content (mmol/g)	Thickness (T, nm), Width (W, nm), Length (L, μ m)	Aspect ratios	ρ_a (mg/cm ³)	Pore vol. (cm ³ /g)	Measured (mL/g)	Measured + Pore vol. (%)	Measured (mL/g)	Measured + Pore vol. (%)	E_p kPa(mg/cm ²)	$\epsilon=80\%$ kPa(mg/cm ²)	E_p kPa(mg/cm ²)	$\epsilon=80\%$ kPa(mg/cm ²)
LCMNF ^b	0.76 (n=1)	T: 1.43 \pm 0.56 (n=35) L: 2.1 \pm 0.65 (n=20)	L/T: 1469	7.1 \pm 1.1	142.7 \pm 19.6	110.3 \pm 2.2	77.3 \pm 1.5	111.9 \pm 13.8	78.4 \pm 9.7	0.6 \pm 0.0	1.6 \pm 0.0	0.4 \pm 0.0	0.1 \pm 0.0
ACNF	1.02 \pm 0.0 (n=2)	T: 1.05 \pm 0.29 (n=70) L: 2.04 \pm 0.58 (n=20)	L/T: 1943	7.3 \pm 0.3	145.4 \pm 5.3	130.9 \pm 0.6	90.0 \pm 0.4	126.5 \pm 3.1	87.0 \pm 2.1	31.6 \pm 4.1	8.0 \pm 0.0	2.5 \pm 0.1	1.4 \pm 0.4
CNF ^c	0.84 \pm 0.1 (n=12)	T: 1.39 \pm 0.37 (n=124) W: 5.66 \pm 0.79 (n=98) L: 1.11 \pm 0.19 (n=44)	W/T: 4 L/T: 799 L/W: 196	6.7 \pm 0.5	150.3 \pm 11.6	132.7 \pm 10.4	88.3 \pm 6.9	117.2 \pm 7.3	78.0 \pm 4.9	13.0 \pm 2.3	6.0 \pm 0.7	1.0 \pm 0.4	0.8 \pm 0.3

^aoCNF had 0.91 mmol/g carboxyls (n=1) and width of 5.54 \pm 0.29 (n=63).

^bLCMNF microfibrils were 3–12 μ m wide and 80–340 μ m long.

^c0.99 \pm 0.26 μ m (n=56) length by TEM; 719 L/T and 177 L/W aspect ratios; the average length of CNFs by AFM is higher than by TEM image analysis (p < 0.05, Welch's T-Test, significant statistical difference).

FTIR of the LC isolate was virtually indiscernible from that of AH powders, that is, confirming the presence of lignin and hemicellulose with the 1516 cm⁻¹ aromatic skeletal vibrations and 1729 cm⁻¹ carbonyl C=O stretching, respectively, the characteristic 897 cm⁻¹ (C₁-O-C₄) glycosidic stretching and 3300 cm⁻¹ backbone O-H stretching peaks of cellulose, and the 1631 cm⁻¹ O-H deformation from adsorbed moisture (Figure 2a). The alkali NaOH treatment seemed to effectively remove lignin, while the 1729 cm⁻¹ shoulder and new 2920 and 2840 cm⁻¹ peaks of CH₂ stretching indicated residual hemicelluloses and possibly glycosylated flavonoids responsible for its off-white appearance. The spectrum of organic-extracted cellulose showed no other compounds, thus implying complete removal of all noncellulosic moieties, while the shoulder at 2840 cm⁻¹ of the aqueous cellulose suggested minor impurities.⁵¹

Nanofibrils by Coupled TEMPO Oxidation and Blending. TEMPO-mediated oxidation under basic conditions (pH 10) at a fixed 5 mmol NaClO per gram of AH isolates converted accessible primary C6 hydroxyls to charged sodium carboxylates (COO-Na⁺).³⁰ Accessible hydroxyls were presumably within the amorphous regions and/or at crystalline-amorphous interfaces, given a heterogeneous reaction on a semicrystalline material.^{30,32,36} The TEMPO reaction time decreased with increasing impurity of the sample attributable to the consumption of oxidants by the non-cellulosics which contained more accessible hydroxyls (Table 1). Despite the lowest purity of the LC sample, the TEMPO/blending resulted in LC nanofibrils (LCNFs) at a notable 88% yield in the supernatant, that is, essentially complete conversion of AHs into water-soluble sugars and water-dispersible LCNFs by sequential hot-water extraction and TEMPO/blending alone. The conversion of alkali cellulose into alkali CNFs (ACNFs) was 91%. Overall, the conversions of LCNFs and ACNFs from crude AH powders were 45.2 and 13.7%, respectively, which were nearly 4 times and slightly higher than the purified cellulose content (ca. 12 wt %). While the LCNF seemingly contained significant lignin, hemicelluloses, and other noncellulosics, the entire conversion of the purest celluloses into aqueous-extracted CNFs and organic-extracted CNFs (oCNFs) at 95 and 97% gravimetric yields, or 11.1 and 11.7% of crude AH, respectively, indicated the increasing purity of the differently isolated celluloses. Still, water-extracted and TEMPO-blended LCNFs were the most streamlined and economical.

The varying visual appearances of the aqueous supernatants corroborated the presence of noncellulosic contents (Figure 3a–c). At the same time, the decreasing visible light transmission was mostly attributable to the nanofibril quantities and qualities (dimensions, surface chemistries, and charges) (Figure 3d,e). Given the direct relationship of increased light scattering as the wavelength approaches the diameter of a particle,⁵² the higher light scattering of the LCNFs and ACNFs was attributable to larger and/or longer nanofibrils. The exceptionally higher scattering of the LCNF supernatant prompted further observation by light microscopy of aqueous and air-dried aliquots, showing additional micro-scale lignin aggregates and 3–12 μ m wide and 80–340 μ m long cellulose microfibrils (Figure 3f–h). The primary supernatant (88%) was further centrifuged (11k rpm, 21.6 kg) to give just 6% LCNFs with the rest or 82% being microfibrils, thus the initially termed LCNF hereon was designated as LC micro-/nanofibrils (LCMNFs) (Table 1). By comparison, both secondary supernatants of the other CNFs and ACNFs contained essentially 100% nanofibrils.

FTIR of the various freeze-dried supernatants all showed dissociated sodium carboxylate peaks at 1612 and 1431 cm⁻¹ (Figure 2b), corroborating TEMPO oxidation of the cellulose hydroxyls. Notably, the C=O stretching of carboxylic acid at 1736 cm⁻¹ on LCNFs and 1725 cm⁻¹ on ACNFs and the 2920 and 2840 cm⁻¹ CH₂ stretching bands and 1247 cm⁻¹ xylan C-O stretching on both LCNFs and ACNFs were reminiscent of hemicellulose moieties.

Conductometric titration of each aqueous supernatant followed protonation with excess HCl. The total surface carboxyl contents were 0.76, 1.02, 0.84, and 0.91 mmol/g for the LCNFs, ACNFs, CNFs, and oCNFs, respectively (Figure 2c and Table 2). Titration of the as-is CNF supernatant at neutral pH 7.5 and in the absence of added HCl showed 0.08 mmol/g surface carboxylic acids (Figure 2d), or 9.5% COOH and 90.5% COO-Na⁺, consistent with the dominant 1612 cm⁻¹ peak of dissociated sodium carboxylates (Figure 2b). While all three CNFs carry surface charges, the unique presence of carboxylic acid peaks observed in the spectra of LCNFs and ACNFs indicated surface-bound hemicellulosic glucuronic acids. The highest 1.02 mmol/g carboxyls on the ACNFs supported this conclusion of additional hemicellulosic carboxyls, and the lowest 0.76 mmol/g carboxyl content on LCNFs was consistent with the shortest reaction time.

The TGA spectra of the organic-extracted cellulose and aqueous cellulose showed similar thermal profiles with

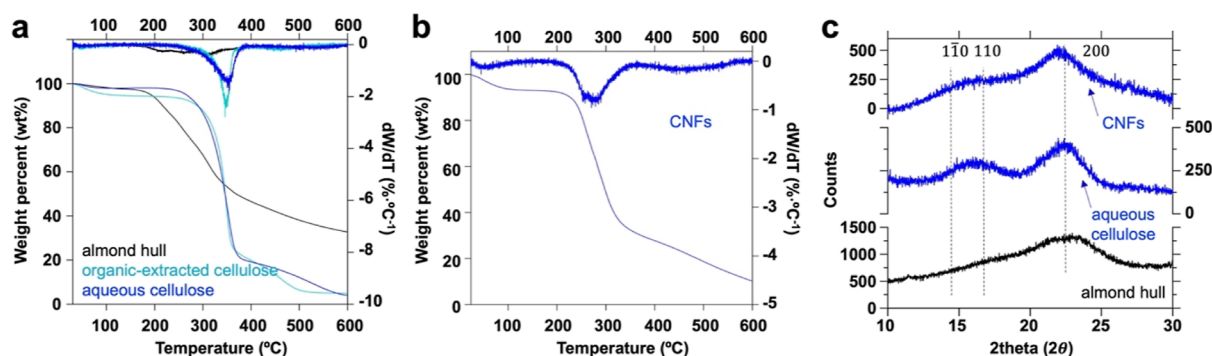


Figure 4. Characterization of AH, purified celluloses, and CNFs: (a) TGA/dTGA of freeze-dried AH powders, organic-extracted cellulose, and aqueous celluloses; (b) TGA/dTGA of freeze-dried CNFs; (c) XRD.

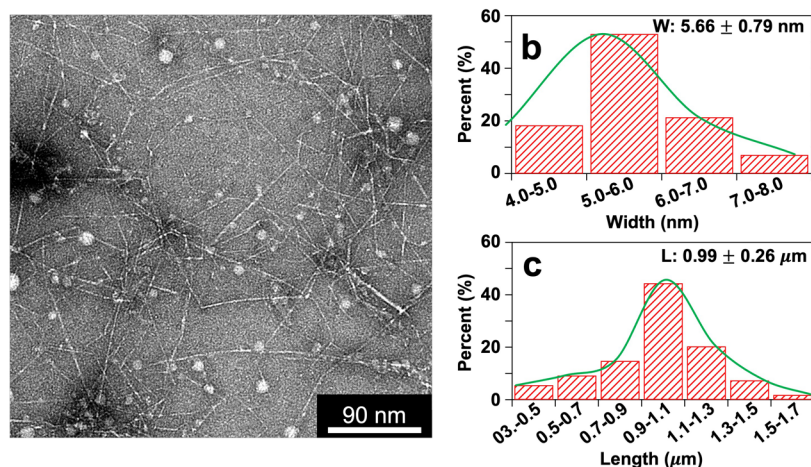


Figure 5. Characterization of TEMPO-oxidized CNFs from aqueous cellulose: (a) TEM image; (b) width and (c) length distributions. Aggregates in (a) are uranyl acetate from negative staining.

significant mass loss at ~ 355 °C (T_{\max}) and $\sim 4\%$ char at 600 °C. Notably, the organic-extracted cellulose was most hygroscopic, releasing $\sim 5\%$ moisture at 150 °C (Figure 4a). The CNFs had higher moisture absorption of 7.1 and 10.2% char but a lowered T_{\max} of 266 °C (Figure 4b). The XRD of CNFs showed monoclinic cellulose 1β peaks at 14.7, 16.8, and 22.7° with a crystallinity index (CrI) of 0.47 versus the 0.58 of aqueous cellulose (Figure 4c). This 11% lower crystallinity of nanocellulose was consistent with the effect of chemical/mechanical defibrillation. By comparison, aqueous-extracted ($\text{NaClO}_2/\text{KOH}$) cellulose from the almond shell showed a 7% decrease from 0.66 to 0.59 CrI for CNFs following identical TEMPO/blending.⁴²

Characterization of Nanofibril Dimensions. The dimensions of CNFs were determined by atomic force microscopy (AFM) and TEM. The TEM widths (W) of oCNFs and CNFs were 5.54 (± 0.29) and 5.66 (± 0.79) nm, respectively (Figure 5a,b and Table 2), showing no statistical difference ($p > 0.05$, Welch's T -test). Organic solvent dewaxing did not cause significant differences in the yields of purified celluloses and their chemical compositions nor the yields and dimensions of their CNFs. Therefore, only CNFs derived from aqueous cellulose without organic extraction were characterized hereon.

For CNFs, ACNFs, and LCNFs, the thicknesses (T) determined via AFM were 1.39 (± 0.37), 1.05 (± 0.29), and 1.43 (± 0.29) nm, and lengths (L), which were more difficult to measure via AFM, were 1.11 (± 0.19), 2.04 (± 0.58), and 2.1

(± 0.65) μm , respectively (Figure 6a–c and Table 2). All CNFs were uniquely anisotropic with a 4:1 width to thickness (W/T) aspect ratio and L/T aspect ratios of 799, 1943, and 1469 for CNFs, ACNFs, and LCNFs, respectively. The much higher L/T anisotropy of the ACNF and LCNFs is consistent with the reduced cellulose chain scission from the consumption of the oxidant by the lignin and hemicelluloses present. Meanwhile, imaging of the LCNF supernatant showed 5–50 nm diameter nanoaggregates which were likely lignin liberated by hypochlorite oxidative cleavage⁵³ and mechanical shearing by blender (Figure 6c). Similar lignin-containing aggregates have been reported via grinding,^{54,55} high-pressure homogenization/microfluidization,⁵⁶ blending/ultrasonication,⁵⁷ acidic deep eutectic solvent/blending,⁵⁸ TEMPO/high-energy fluidization,⁵⁹ and screw extrusion.⁶⁰

In order to calculate the CNF surface charge density from TEMPO oxidation, several assumptions were made about the crystalline surface planes of CNFs based on previous work.⁶¹ First, the surface plane along the width corresponds to the hydroxyl-rich and hydrophilic 110 lattice plane exposed on both top and bottom surfaces. Therefore, the 1.39 nm thickness of CNFs corresponds to the (more hydrophobic) 200 crystal lattice plane. Assuming a rhomboidal cross-section,⁴⁷ the total C6 surface hydroxyl content per exposed AGU on the top and bottom of CNFs was calculated to be 0.584 mol/mol. Hence, the 0.84 mmol/g charges or 0.136 mol/mol carboxyl/AGU on CNFs is equivalent of a 23% C6 hydroxyl-to-carboxyl conversion by TEMPO oxidation. The

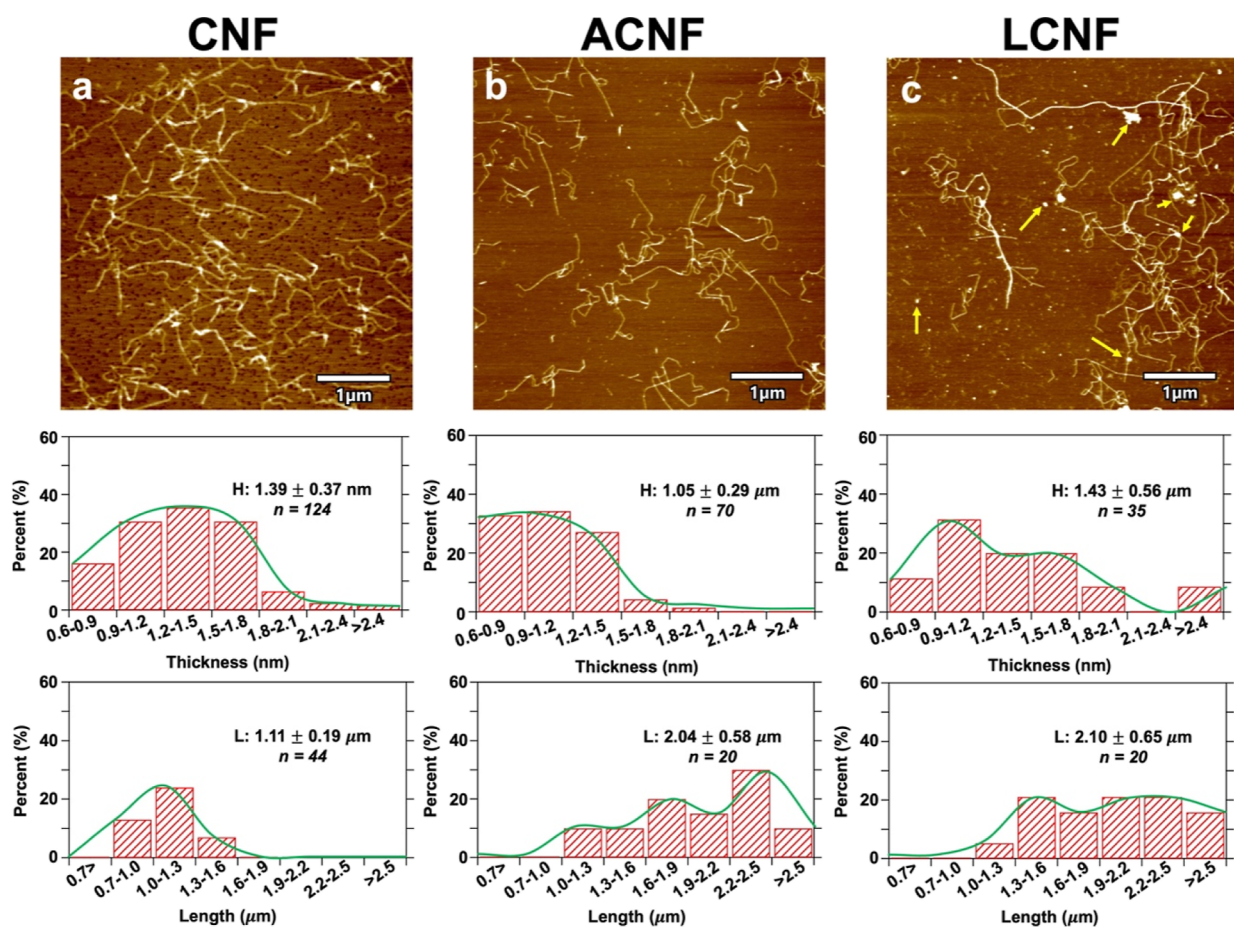


Figure 6. AFM of (a) CNF, (b) ACNF, and (c) LCNF (0.0005 w/v %) with the corresponding thickness and length distributions given below. Lignin nanoparticles are indicated by arrows in (c).

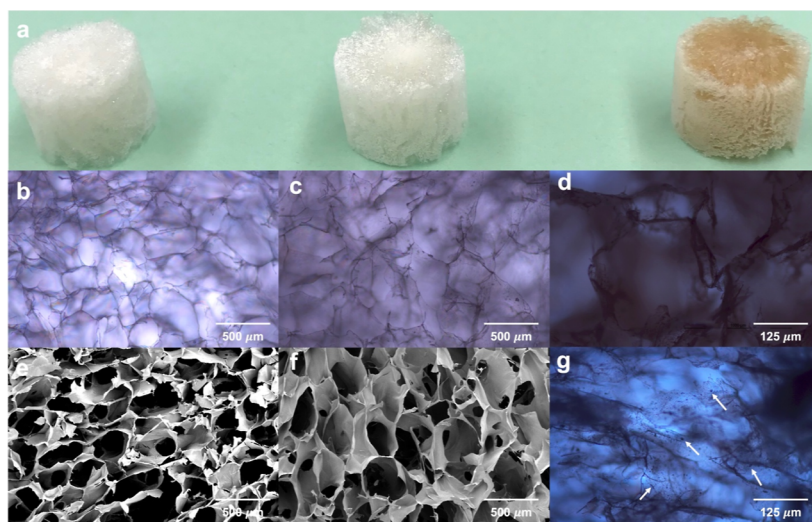


Figure 7. AH aerogels: (a) photographic images of CNF, ACNF, and LCMNF aerogels (left to right); (b–d) optical microscopic images of the corresponding radial cross-sections from the corresponding aerogels above in (a); (e,f) SEM images of radial and longitudinal sections (<1 mm) of the CNF aerogel; (g) cross-section at 45° orientation of the LCMNF aerogel with arrows pointing to lignin aggregates in cell walls.

same TEMPO/blending of aqueous-extracted almond shell cellulose produced 5.2 nm wide, 1.2 nm thick, and $\sim 1 \mu\text{m}$ long CNFs at 92% yield, that is, similar 4.3 W/T lateral anisotropy, but higher 1.3 mmol/g (0.211 COOH/AGU) surface carboxyls and 61% C6 hydroxyl-to-carboxyl conversion.⁴² Therefore, while the AH and shell from the same variety

produced CNFs in similar dimensions and yields, the less-crystalline AH (0.58 vs 0.66 CrI) produced CNFs with lower crystallinity (0.47 vs 0.59 CrI), surface carboxyl (0.91 vs 1.3 mmol/g), and C6 hydroxyl-to-carboxyl conversion (23 vs 61%) in comparison to almond shell CNF from the same TEMPO/blending process.

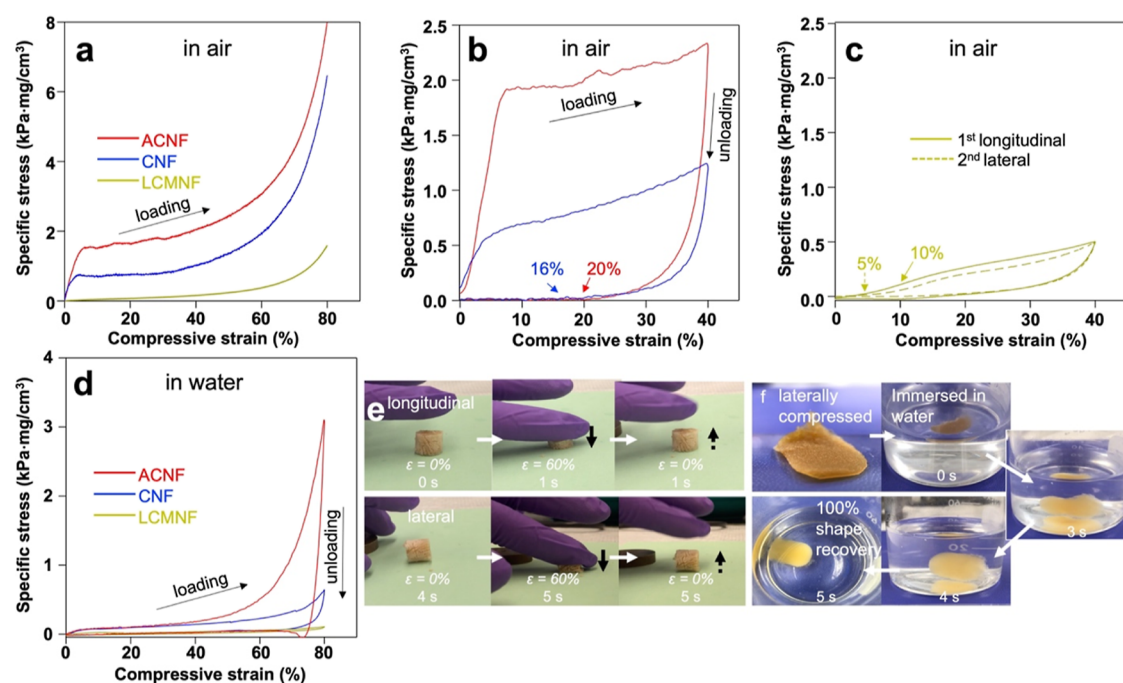


Figure 8. Uniaxial compressive stress–strain (σ – ϵ) properties of aerogels (10 mm height and 14 mm diameter) from 0.6 w/v % CNF, ACNF, and LCMNF: (a) loading to 80% strain in air; (b,c) loading–unloading from 0 to 40% strain in air; (d) loading–unloading from 0 to 80% in water; (e) compression and recovery of dry LCMNF aerogel in the longitudinal (top) and lateral (bottom) directions; (f) LCMNF aerogel wet recovery and resilience following hand compressions ($\epsilon \geq 95\%$).

Effect of Nanofibril Qualities on the Properties of Aerogels. Slow and isotropic freezing ($-20\text{ }^{\circ}\text{C}$, overnight) of the various supernatants and freeze-drying produced aerogels with significant ($>95\%$) volumetric retention (Figure 7a). Optical microscopy of the radial cross-sections of aerogels revealed cellular structures with sub-millimeter size pores surrounded by semitransparent super-thin walls (Figure 7b–d). SEM imaging of the cross-sections of CNF aerogel confirmed isotropic and interconnected open cells with widths of $201\text{ }\mu\text{m}$ (± 54) and $169\text{ }\mu\text{m}$ (± 72) in the, respective, radial and longitudinal directions (Figure 7e,f). Notably, lignin aggregates were also observed as surface-bound or interfibrillar-embedded in the cell walls of the LCMNF aerogel (Figure 7g).

All three types of aerogels had ultra-low density (6.7 – 7.3 mg/cm^3), ultra-high porosity (99.6 – 99.7%), and ultra-high pore volume (143 – $150\text{ cm}^3/\text{g}$) (Table 2), all statistically equal ($p > 0.05$, one-way ANOVA). All three aerogels were amphiphilic superabsorbents of polar water (110 – 133 mL/g) and nonpolar decane (112 – 127 mL/g). The CNF aerogels were slightly more hydrophilic, absorbing 133 mL/g water and 117 mL/g decane, whereas the ACNF and LCMNF aerogels were similarly hydrophilic and hydrophobic. The polar and nonpolar liquid absorption values were 77 – 90% and 78 – 87% of the pore volumes, respectively (Table 2), signifying the open-cell nature of the majority of pores in these aerogels. The amphiphilic surfaces of the cellular walls, on the other hand, supported the notion that TEMPO/blending exposed both the hydrophilic and hydrophobic crystalline surfaces of nanofibrils as proposed earlier and these nanofibrils self-assemble randomly to expose both hydrophilic and hydrophobic surfaces.

Compression stress–strain curves of aerogels obtained in the height direction of the cylindrical samples showed a linear

elastic regime of bending of the cell walls ($\epsilon \leq 10\%$), a stress plateau of progressive cell collapse ($10\% \leq \epsilon \leq 60\%$) and, ultimately, the complete collapse of all cell walls ($\epsilon \leq 80\%$) (Figure 8a), typical of 3D cellular solids.⁶² While all three aerogels had similar densities, the specific modulus ($E_{\rho}, \epsilon < 2\%$) of the ACNF aerogel was $31.6\text{ kPa}/(\text{mg}/\text{cm}^3)$ or 2.4 times of the $13.1\text{ kPa}/(\text{mg}/\text{cm}^3)$ of the CNF aerogel, yet had $8.0\text{ kPa}/(\text{mg}/\text{cm}^3)$ strength or just a third higher than the $6.0\text{ kPa}/(\text{mg}/\text{cm}^3)$ of CNF aerogel at 80% strain (Table 2). The LCMNF aerogel showed drastically lower 0.6 and $1.6\text{ kPa}/(\text{mg}/\text{cm}^3)$ specific modulus and strength, respectively, only 2 and 20% of the strongest ACNF aerogel. However, while extremely tough, the ACNF and CNF aerogels only recovered to 20 and 16% strain upon unloading (0 kPa stress) after 40% strain (Figure 8b). Conversely, the LCMNF aerogel could recover to 90% height and 95% width from sequential longitudinal-then-lateral, loading–unloading to 40% strain (Figure 8c).

In water, ACNF and CNF aerogels exhibited dramatically decreased wet compressive modulus and strength by approximately 1 order of magnitude. Yet, LCMNF aerogel with least-dry compressive modulus and strength retained most of its modulus but lost nearly all its strength in water (Figure 8d and Table 2). The dramatic reduction in the mechanical performances of all aerogels from dry to wet states indicated the dominance of intracellular wall interfibrillar polar and hydrogen bonding since water is highly effective in breaking these hydrophilic interfacial CNF associations. Still, the ACNF aerogels had the highest wet strength, attributable to the superior self-assembly of ACNF with highest surface hemi-cellulosic carboxyls (1.02 mmol/g) and highest L/T ratio.

The LCMNF aerogel was the most dry-resilient and shape-recoverable in air, attributable to the microfibril cell wall composition (Figure 8e). These microfibril aerogels showed

impressive wet resilience by remaining intact in water for >14 days and had water-activated shape recovery (Figure 8f). By comparison, both ACNF and CNF aerogels prepared herein disintegrated upon being submerged in water in 2 days. The unique wet stability of the LCMNF aerogels suggested the benefiting role of the noncellulosics by serving as intermicrofibril and internanofibril cementing agents. Previously, residual lignin moieties enhanced the wet mechanical performance of CNF films.^{56,63} The presence of residual lignin and hemicelluloses on the LCMNF surfaces may enhance interfibrillar bonding or hydrophobic and/or hydrophilic interactions.

Both the 13.1 kPa/(mg/cm³) specific modulus and 6.0 kPa/(mg/cm³) strength of the CNF aerogel were 2 times higher than those (6.7 and 3.1) of TEMPO-CNF aerogel prepared from organic-extracted rice straw CNF by the same TEMPO/blending process.⁴⁴ The 2-fold higher stiffness of the AH aerogel was attributable to the uniquely anisotropic CNF cross-sectional dimensions of nearly 3-fold larger hydroxyl-rich and hydrogen-bonding width (Figure 6d). Only a rice straw CNF aerogel chemically cross-linked with MDI had a higher 18.2 kPa/(mg/cm³) specific modulus and 5.7 kPa/(mg/cm³) strength.⁶⁴ Remarkably, even the ACNF aerogel was 1.7 times stiffer [31.6 kPa/(mg/cm³)] and 1.4 times stronger [8.0 kPa/(mg/cm³)] than the MDI-crosslinked aerogel, again attributable to the ultrahigh-aspect-ratio ACNFs.

As final remarks, this study has established a process for combining sugar extraction with streamlined production of nanocelluloses from AH, a significant agricultural byproduct, that synergistically adds value to this under-valued biomass source. Specifically, concurrent extraction of valuable free sugars and production of high value-added CNFs result in two commercially viable products: (1) clean, food-grade sugar and (2) CNFs with unique attributes for self-assembly into wet-resilient aerogels for bio-degradable sponges and super-absorbents. This study has demonstrated a process roadmap to deliver significant value to under-utilized AH in the form of nanocelluloses and sugar coproducts, particularly in terms of sustainable industrially scalable chemical-mechanical processing of upcycled crude LC into CNFs of diverse qualities using TEMPO oxidation with minimal environmental footprint.^{65,66}

AUTHOR INFORMATION

Corresponding Author

You-Lo Hsieh – *Biological and Agricultural Engineering, University of California, Davis, California 95616, United States*; orcid.org/0000-0003-4795-260X; Email: yhhsieh@ucdavis.edu

Authors

Gabriel D. Patterson – *Bioproducts Research Unit, WRRC, ARS-USDA, Albany, California 94710, United States*; *Biological and Agricultural Engineering, University of California, Davis, California 95616, United States*; orcid.org/0000-0002-1015-9192

William J. Orts – *Bioproducts Research Unit, WRRC, ARS-USDA, Albany, California 94710, United States*; orcid.org/0000-0001-7716-7296

James D. McManus – *Bioproducts Research Unit, WRRC, ARS-USDA, Albany, California 94710, United States*

Complete contact information is available at:

<https://pubs.acs.org/10.1021/acsagscitech.2c00264>

Author Contributions

G.D.P.: experimental execution, data analysis, validation, presentation, and writing—original draft, revision. **G.D.P. and Y.L.H.:** conceptualization and design of methodology and visualization. **Y.L.H.:** funding acquisition. **G.D.P., J.D.M., W.J.O., and Y.L.H.:** final writing, review, and editing. **J.D.M. and W.J.O.:** additional resources and supervision.

Notes

The authors declare no competing financial interest.

ACKNOWLEDGMENTS

Financial support for this research from the United States Department of Agriculture (USDA) Western Sun Grant, and the Jastro Shields Research Award, University of California, Davis, is greatly appreciated.

ABBREVIATIONS

AH, almond hull; AGU, anhydroglucose unit; CNF, aqueous-extracted cellulose nanofibril; oCNF, organic-extracted cellulose nanofibril; ACNF, alkali cellulose nanofibril; LCNF, lignocellulose nanofibril; LCMNF, lignocellulose micro-/nanofibril; TEMPO, 2,2,6,6-tetramethylpiperidine-1-oxyl; NaClO, sodium hypochlorite; AFM, atomic force microscopy; TEM, transmission electron microscopy; SEM, scanning electron microscopy; *T*, thickness; *W*, width; *L*, length

REFERENCES

- (1) French, A. D.; Bertoniere, N. R.; Brown, R.; Chanzy, H.; Gray, D.; Hattori, K.; Glasser, W. Cellulose. *Encyclopedia of Polymer Science and Technology*, 2003.
- (2) Dufresne, A. Nanocellulose: a new ageless bionanomaterial. *Materials Today* **2013**, *16*, 220–227.
- (3) Dong, X. M.; Revol, J.-F.; Gray, D. G. Effect of microcrystallite preparation conditions on the formation of colloid crystals of cellulose. *Cellulose* **1998**, *5*, 19–32.
- (4) Plappert, S. F.; Liebner, F. W.; Konnerth, J.; Nedelec, J.-M. Anisotropic nanocellulose gel–membranes for drug delivery: Tailoring structure and interface by sequential periodate–chlorite oxidation. *Carbohydr. Polym.* **2019**, *226*, 115306.
- (5) Meftahi, A.; Samyn, P.; Geravand, S. A.; Khajavi, R.; Alibkshhi, S.; Bechelany, M.; Barhoum, A. Nanocelluloses as skin biocompatible materials for skincare, cosmetics, and healthcare: Formulations, regulations, and emerging applications. *Carbohydr. Polym.* **2022**, *278*, 118956.
- (6) Mattoso, L. H. C.; Medeiros, E. S.; Baker, D. A.; Avloni, J.; Wood, D. F.; Orts, W. J. Electrically conductive nanocomposites made from cellulose nanofibrils and polyaniline. *J. Nanosci. Nanotechnol.* **2009**, *9*, 2917–2922.
- (7) Orts, W. J.; Godbout, L.; Marchessault, R. H.; Revol, J.-F. Enhanced Ordering of Liquid Crystalline Suspensions of Cellulose Microfibrils: A Small Angle Neutron Scattering Study. *Macromolecules* **1998**, *31*, 5717–5725.
- (8) International Nuts and Dried Fruits Council (INC), *Statistical Yearbook2020/2021*. <http://www.nutfruit.org> (accessed April 3, 2022).
- (9) Almond Board of California (ABC), *Almond Almanac2020*<http://www.almonds.com> (accessed December 27, 2020).
- (10) California Department of Food and Agriculture (CDFA), *Agricultural Statistics Review2018/2019*<http://www.cdfa.ca.gov> (accessed January 02, 2021).
- (11) United States Department of Agriculture (USDA). *California Agricultural Statistics Review 2016–2017*, Livestock and Dairy, 2017, pp 83–88.
- (12) Pan, Z.; Zhang, R.; Zicari, S. *Integrated Processing Technologies for Food and Agricultural By-Products*; Academic Press, 2019.

- (13) Cruess, W.; et al. Almond meats and hulls: new and improved uses for larger-sized meats and for hulls subjects of investigations. *Calif. Agric.* **1949**, *3*, 6–12.
- (14) Velasco, M.; Schoner, C.; Lofgreen, G.; et al. Composition and feeding value of almond hulls and hull-shell meal. *Calif. Agric.* **1965**, *19*, 12–14.
- (15) Sequeira, R. M.; Lew, R. B. The carbohydrate composition of almond hulls. *J. Agric. Food Chem.* **1970**, *18*, 950–951.
- (16) Saura-Calixto, F.; Canellas, J.; Garcia-Raso, J. Contents of detergent-extracted dietary fibers and composition of hulls, sheels, and teguments of almonds (*Prunus amygdalus*). *J. Agric. Food Chem.* **1983**, *31*, 1255–1259.
- (17) Aguilar, A. A.; Smith, N. E.; Baldwin, R. L. Nutritional value of almond hulls for dairy cows. *J. Dairy Sci.* **1984**, *67*, 97–103.
- (18) Reed, B. A.; Brown, D. L. Almond hulls in diets for lactating goats: effects on yield and composition of milk, feed intake, and digestibility. *J. Dairy Sci.* **1988**, *71*, 530–533.
- (19) DePeters, E. J.; Fadel, J. G.; Arana, M. J.; Ohanesian, N.; Etchebarne, M. A.; Hamilton, C. A.; Hinders, R. G.; Maloney, O.; Old, T. J.; Riordan, H.; Perez-Monti, J. W.; Pareas, J. W. Variability in the Chemical Composition of Seventeen Selected By-Product Feedstuffs Used by the California Dairy Industry. *The Professional Animal Scientist* **2000**, *16*, 69–99.
- (20) Yalchi, T.; Kargar, S.; et al. Chemical composition and in situ ruminal degradability of dry matter and neutral detergent fiber from almond hulls. *J. Food Agric. Environ.* **2010**, *8*, 781–784.
- (21) Offeman, R. D.; Dao, G. T.; Holtman, K. M.; Orts, W. J. Leaching behavior of water-soluble carbohydrates from almond hulls. *Ind. Crops Prod.* **2015**, *65*, 488–495.
- (22) Holtman, K. M.; Offeman, R. D.; Franqui-Villanueva, D.; Bayati, A. K.; Orts, W. J. Countercurrent extraction of soluble sugars from almond hulls and assessment of the bioenergy potential. *J. Agric. Food Chem.* **2015**, *63*, 2490–2498.
- (23) United States Department of Agriculture USDA, *National Agricultural Statistics Service – Pacific Region (NASS/PR) 2020 Acreage Report*, 2022. <http://www.nass.usda.gov> (accessed December 27, 2020).
- (24) Wang, J.; Singh, A. K.; Kong, F.; Kim, W. K. Effect of almond hulls as alternative ingredients on broiler performance, nutrient digestibility and cecal microbiota diversity. *Poult. Sci.* **2021**, *100*, 100853.
- (25) Palma, L.; Fernández-Bayo, J.; Putri, F.; VanderGheynst, J. S. Almond by-product composition impacts the rearing of black soldier fly larvae and quality of the spent substrate as a soil amendment. *J. Sci. Food Agric.* **2020**, *100*, 4618–4626.
- (26) Rabinowitz, I. Edible Food Produced Such as Sports Beverages, Health Drinks, Fruit Bars, Jams and Jellies, 2002. U.S. Patent no. 20020132031 A1.
- (27) Rubilar, M.; Pinelo, M.; Shene, C.; Sineiro, J.; Nuñez, M. J. Separation and HPLC-MS identification of phenolic antioxidants from agricultural residues: almond hulls and grape pomace. *J. Agric. Food Chem.* **2007**, *55*, 10101–10109.
- (28) Isfahlan, A. J.; Mahmoodzadeh, A.; Hasanzadeh, A.; Heidari, R.; Jamei, R. Antioxidant and antiradical activities of phenolic extracts from Iranian almond (*Prunus amygdalus* L.) hulls and shells. *Turk. J. Biol.* **2010**, *34*, 165–173.
- (29) An, J.; Liu, J.; Liang, Y.; Ma, Y.; Chen, C.; Cheng, Y.; Peng, P.; Zhou, N.; Zhang, R.; Addy, M.; Chen, P.; Liu, Y.; Huang, G.; Ren, D.; Ruan, R. Characterization, bioavailability and protective effects of phenolic-rich extracts from almond hulls against pro-oxidant induced toxicity in Caco-2 cells. *Food Chem.* **2020**, *322*, 126742.
- (30) Saito, T.; Kimura, S.; Nishiyama, Y.; Isogai, A. Cellulose nanofibers prepared by TEMPO-mediated oxidation of native cellulose. *Biomacromolecules* **2007**, *8*, 2485–2491.
- (31) Rosa, M. F.; Medeiros, E. S.; Malmonge, J. A.; Gregorski, K. S.; Wood, D. F.; Mattoso, L. H. C.; Glenn, G.; Orts, W. J.; Imam, S. H. Cellulose nanowhiskers from coconut husk fibers: Effect of preparation conditions on their thermal and morphological behavior. *Carbohydr. Polym.* **2010**, *81*, 83–92.
- (32) Lu, P.; Hsieh, Y.-L. Preparation and properties of cellulose nanocrystals: Rods, spheres, and network. *Carbohydr. Polym.* **2010**, *82*, 329–336.
- (33) Lu, P.; Hsieh, Y.-L. Cellulose isolation and core–shell nanostructures of cellulose nanocrystals from chardonnay grape skins. *Carbohydr. Polym.* **2012**, *87*, 2546–2553.
- (34) Jiang, F.; Hsieh, Y.-L. Cellulose nanocrystal isolation from tomato peels and assembled nanofibers. *Carbohydr. Polym.* **2015**, *122*, 60–68.
- (35) Lu, P.; Hsieh, Y.-L. Preparation and characterization of cellulose nanocrystals from rice straw. *Carbohydr. Polym.* **2012**, *87*, 564–573.
- (36) Jiang, F.; Han, S.; Hsieh, Y.-L. Controlled defibrillation of rice straw cellulose and self-assembly of cellulose nanofibrils into highly crystalline fibrous materials. *RSC Adv.* **2013**, *3*, 12366–12375.
- (37) Patterson, G.; Hsieh, Y.-L. Tunable dialdehyde/dicarboxylate nanocelluloses by stoichiometrically optimized sequential periodate–chlorite oxidation for tough and wet shape recoverable aerogels. *Nanoscale Adv.* **2020**, *2*, 5623–5634.
- (38) Wang, D.; Yu, H.; Fan, X.; Gu, J.; Ye, S.; Yao, J.; Ni, Q. High Aspect Ratio Carboxylated Cellulose Nanofibers Cross-linked to Robust Aerogels for Superabsorption-Flocculants: Paving Way from Nanoscale to Macroscale. *ACS Appl. Mater. Interfaces* **2018**, *10*, 20755–20766.
- (39) Mandal, A.; Chakrabarty, D. Isolation of nanocellulose from waste sugarcane bagasse (SCB) and its characterization. *Carbohydr. Polym.* **2011**, *86*, 1291–1299.
- (40) Messa, L. L.; Faez, R.; Hsieh, Y.-L. Phosphorylated cellulose nanofibrils from sugarcane bagasse with pH tunable gelation. *Carbohydr. Polym. Technol. Appl.* **2021**, *2*, 100085.
- (41) Yang, X.; Han, F.; Xu, C.; Jiang, S.; Huang, L.; Liu, L.; Xia, Z. Effects of preparation methods on the morphology and properties of nanocellulose (NC) extracted from corn husk. *Ind. Crops Prod.* **2017**, *109*, 241–247.
- (42) Fukuda, J.; Hsieh, Y.-L. Almond shell nanocellulose: Characterization and self-assembling into fibers, films, and aerogels. *Ind. Crops Prod.* **2022**, *186*, 115188.
- (43) Kanai, N.; Nishimura, K.; Umetani, S.; Saito, Y.; Saito, H.; Oyama, T.; Kawamura, I. Upcycling of Waste Hop Stems into Cellulose Nanofibers: Isolation and Structural Characterization. *ACS Agric. Sci. Technol.* **2021**, *1*, 347–354.
- (44) Jiang, F.; Hsieh, Y.-L. Amphiphilic superabsorbent cellulose nanofibril aerogels. *J. Mater. Chem. A* **2014**, *2*, 6337–6342.
- (45) Gu, J.; Hsieh, Y.-L. Alkaline Cellulose Nanofibrils from Streamlined Alkali Treated Rice Straw. *ACS Sustainable Chem. Eng.* **2017**, *5*, 1730–1737.
- (46) Segal, L.; Creely, J. J.; Martin, A. E.; Conrad, C. M. An Empirical Method for Estimating the Degree of Crystallinity of Native Cellulose Using the X-Ray Diffractometer. *Text. Res. J.* **1959**, *29*, 786–794.
- (47) Helbert, W.; Nishiyama, Y.; Okano, T.; Sugiyama, J. Molecular Imaging of *Halocynthia papillosa* Cellulose. *J. Struct. Biol.* **1998**, *124*, 42–50.
- (48) Ganster, J.; Fink, H.-P. Physical Constants of Cellulose. *The Wiley Database of Polymer Properties* **1999**, bra036.
- (49) Deshwal, B. R.; Jo, H.-D.; Lee, H.-K. Reaction kinetics of decomposition of acidic sodium chlorite. *Can. J. Chem. Eng.* **2004**, *82*, 619–623.
- (50) Kolar, J. J.; Lindgren, B. O.; Pettersson, B. Chemical reactions in chlorine dioxide stages of pulp bleaching. *Wood Sci. Technol.* **1983**, *17*, 117–128.
- (51) Ahlgren, P. A.; Goring, D. A. I. Removal of Wood Components During Chlorite Delignification of Black Spruce. *Can. J. Chem.* **1971**, *49*, 1272–1275.
- (52) Carr, M. E.; Shen, L. L.; Hermans, J. Mass-length ratio of fibrin fibers from gel permeation and light scattering. *Biopolymers* **1977**, *16*, 1–15.
- (53) Liu, S.; Bai, L.; van Muyden, A. P.; Huang, Z.; Cui, X.; Fei, Z.; Li, X.; Hu, X.; Dyson, P. J. Oxidative cleavage of β -O-4 bonds in lignin

model compounds with a single-atom Co catalyst. *Green Chem.* **2019**, *21*, 1974–1981.

(54) Chen, Y.; Fan, D.; Han, Y.; Lyu, S.; Lu, Y.; Li, G.; Jiang, F.; Wang, S. Effect of high residual lignin on the properties of cellulose nanofibrils/films. *Cellulose* **2018**, *25*, 6421–6431.

(55) Peng, Y.; Nair, S. S.; Chen, H.; Yan, N.; Cao, J. Effects of Lignin Content on Mechanical and Thermal Properties of Polypropylene Composites Reinforced with Micro Particles of Spray Dried Cellulose Nanofibrils. *ACS Sustainable Chem. Eng.* **2018**, *6*, 11078–11086.

(56) Imani, M.; Ghasemian, A.; Dehghani-Firouzabadi, M. R.; Afra, E.; Borghei, M.; Johansson, L. S.; Gane, P. A. C.; Rojas, O. J. Coupling nanofibril lateral size and residual lignin to tailor the properties of lignocellulose films. *Adv. Mater. Interfaces* **2019**, *6*, 1900770.

(57) Han, X.; Bi, R.; Oguzlu, H.; Takada, M.; Jiang, J.; Jiang, F.; Bao, J.; Saddler, J. N. Potential To Produce Sugars and Lignin-Containing Cellulose Nanofibrils from Enzymatically Hydrolyzed Chemi-Thermomechanical Pulps. *ACS Sustainable Chem. Eng.* **2020**, *8*, 14955–14963.

(58) Jiang, J.; Carrillo-Enríquez, N. C.; Oguzlu, H.; Han, X.; Bi, R.; Song, M.; Saddler, J. N.; Sun, R.-C.; Jiang, F. High Production Yield and More Thermally Stable Lignin-Containing Cellulose Nanocrystals Isolated Using a Ternary Acidic Deep Eutectic Solvent. *ACS Sustainable Chem. Eng.* **2020**, *8*, 7182–7191.

(59) Imani, M.; Dimic-Misic, K.; Tavakoli, M.; Rojas, O. J.; Gane, P. A. C. Coupled Effects of Fibril Width, Residual and Mechanically Liberated Lignin on the Flow, Viscoelasticity, and Dewatering of Cellulosic Nanomaterials. *Biomacromolecules* **2020**, *21*, 4123–4134.

(60) Lu, H.; Zhang, L.; Yan, M.; Wang, K.; Jiang, J. Screw extrusion pretreatment for high-yield lignocellulose nanofibrils (LCNF) production from wood biomass and non-wood biomass. *Carbohydr. Polym.* **2022**, *277*, 118897.

(61) Okita, Y.; Saito, T.; Isogai, A. Entire Surface Oxidation of Various Cellulose Microfibrils by TEMPO-Mediated Oxidation. *Biomacromolecules* **2010**, *11*, 1696–1700.

(62) Gibson, L. J. Biomechanics of cellular solids. *J. Biomech.* **2005**, *38*, 377–399.

(63) Nair, S. S.; Yan, N. Effect of high residual lignin on the thermal stability of nanofibrils and its enhanced mechanical performance in aqueous environments. *Cellulose* **2015**, *22*, 3137–3150.

(64) Jiang, F.; Hsieh, Y.-L. Cellulose Nanofibril Aerogels: Synergistic Improvement of Hydrophobicity, Strength, and Thermal Stability via Cross-Linking with Diisocyanate. *ACS Appl. Mater. Interfaces* **2017**, *9*, 2825–2834.

(65) Li, Q.; McGinnis, S.; Sydnor, C.; Wong, A.; Rennecker, S. Nanocellulose Life Cycle Assessment. *ACS Sustainable Chem. Eng.* **2013**, *1*, 919–928.

(66) Gallo Stampino, P.; Riva, L.; Punta, C.; Elegir, G.; Bussini, D.; Dotelli, G. Comparative Life Cycle Assessment of Cellulose Nanofibres Production Routes from Virgin and Recycled Raw Materials. *Molecules* **2021**, *26*, 2558.

Recommended by ACS

Rapid Colorimetric Detection of Thiabendazole Based on Its Inhibition Effect on the Peroxidase Mimetic Activity of Ag-MoS₂ Nanozyme

Menbere Leul Mekonnen, Ebrahim Mama Abda, *et al.*

JANUARY 03, 2023

ACS AGRICULTURAL SCIENCE & TECHNOLOGY

READ 

Design, Synthesis, Inhibitory Activity, and Molecular Modeling of Novel Pyrazole-Furan/Thiophene Carboxamide Hybrids as Potential Fungicides Targeting Succinate Deh...

Wenjing Jiang, Xiaorong Tang, *et al.*

DECEMBER 23, 2022

JOURNAL OF AGRICULTURAL AND FOOD CHEMISTRY

READ 

Fault Tolerance Optimization of a Lithium Battery Pack Having a Damaged Unit

Fusheng Gu, Zhenzhe Li, *et al.*

AUGUST 22, 2022

ACS OMEGA

READ 

Using Pet Food as the Subject to Investigate the Effectiveness of Whole-Genome Sequencing in the Authentication of Highly Processed Complex Food

Xuechen Zhu, Jeremy S. Edwards, *et al.*

JANUARY 06, 2023

ACS FOOD SCIENCE & TECHNOLOGY

READ 

Get More Suggestions >